Assessment of Kappa Values in the Chilean Subduction Zone for Interface and In-Slab Events

Ignacio Pozo[1], Gonzalo Montalva[*1], and Matthew Miller[1]

Abstract

One way to study the physical process that occurs behind earthquakes and how they affect different sites depending on the source type and the geological structure of the site is the shape of the Fourier spectrum. A parameter related to the shape of the spectrum is the spectral decay factor—kappa (κ), which characterizes how the amplitude of the Fourier acceleration spectrum decays at high frequencies. The parameter κ can be important in the characterization and estimation of the surface seismic demand, being useful in, for example, the adjustment of ground-motion prediction equations. We calculate the values of κ and its site component κ_0 from 36 seismic stations of the National Seismological Network of Chile to determine the dependence that this parameter has to the site conditions as well as to the properties of the path in which greater values of κ are observed for subduction earthquakes that occur in the interface between the Nazca and the South American plates, compared with the values obtained from events occurring inside the subducting plate, known as in-slab earthquakes. We find that κ_0, calculated using the hypocentral distance correlates more closely with the site fundamental frequency f_0, rather than the commonly used V_{S30} (time-averaged shear-wave velocity in the top 30 m). Our kappa value results are field estimates of near-surface attenuation, which can be used to calculate the minimum site-specific damping or crustal attenuation in seismological models that have a strong impact on seismic site characterization, particularly, in subduction settings.

Cite this article as Pozo, I., G. Montalva, and M. Miller (2022). Assessment of Kappa Values in the Chilean Subduction Zone for Interface and In-Slab Events, *Seismol. Res. Lett.* **94**, 385–398, doi: 10.1785/0220220018.

Introduction

The κ parameter, introduced by Anderson and Hough (1984), is the slope that characterizes the decay of the Fourier spectrum at high frequencies. It is a parameter commonly used in the field of engineering seismology, so it is important to know and understand the ranges of values that it can have and the physical properties of the medium it represents. This decay parameter is mainly associated with two components (equation 1)—one related to the site (κ_0) and the other to the path (κ_R). The former, introduced by Hanks (1982), is commonly linked to the physical meaning of κ, whereas the component associated with the trajectory (source–station distance) is related to a frequency-independent quality factor Q, which represents the regional attenuation. Although several studies have shown that the parameter Q is a function of the frequency (Aki, 1980; Havskov *et al.*, 2016; Darragh *et al.*, 2019; Haendel *et al.*, 2020), the condition that Q is independent of frequency is one of the main assumptions of the methodology proposed by Anderson and Hough (1984). For this reason, in this work, this condition is assumed the same as in other studies using this method (Ktenidou *et al.*, 2015; Neighbors *et al.*, 2015; Park *et al.*, 2020; Ji *et al.*, 2021).

$$\kappa(R) = \kappa_0 + \kappa_R \times R. \tag{1}$$

The κ parameter can be used within the context of ground-motion predictive equations to represent the surface attenuation (in the uppermost kilometers of the crust) of seismic waves, considering it as an input parameter in the equations of motion either implicitly, as in most studies (Toro *et al.*, 1997; Campbell, 2003) taking it as part of the uncertainty of the results, and explicitly (Laurendeau *et al.*, 2013; Bora *et al.*, 2017). In addition to using it to make adjustments of these equations for different sites, through its relationship with the time-averaged shear-wave velocity in the top 30 m V_{S30} (Cotton *et al.*, 2006), it can also provide a constraint for the damping parameter $D_{\min}$ (Xu *et al.*, 2020). Additional to the methodology established by Anderson and Hough (1984), using the Fourier acceleration spectrum of the S wave, κ can be calculated through

1. Departamento de Ingeniería Civil, Universidad de Concepción, Concepción, Chile, https://orcid.org/0000-0001-8598-7120 (GM)

*Corresponding author: gmontalva@udec.cl

© Seismological Society of America

Downloaded from http://pubs.geoscienceworld.org/ssa/srl/article-pdf/94/1/385/5756885/srl-2022018.1.pdf
by Universidad de Concepcion, gmontalva

other methods, such as direct measurement from the site transfer function or indirectly through the response spectra generated in a stochastic way (Silva and Darragh, 1995; Drouet *et al.*, 2010). The different methods to determine this parameter have been compiled by Ktenidou *et al.* (2014), who summarize the existing different methodologies in the literature along with the different applications of the parameter κ. There are several studies about kappa in different seismic zones of the world (Bora *et al.*, 2017; Mayor *et al.*, 2018); however, for the Chilean subduction zone we only find the works done by Neighbors *et al.* (2015) and Cabas *et al.* (2015). Both the studies analyze the kappa values from local arrays in the Biobío region. Studies about κ are either focus on the analysis of the parameter itself (Ktenidou *et al.*, 2013; Neighbors *et al.*, 2015; Lai *et al.*, 2016), whereas others use it as a proxy for site effects in different areas of the world (Fu and Li, 2016; Pilz and Fäh, 2017). This work computes values of κ and its components (κ_0 and κ_R) for each of 36 stations of the national seismic network to study the relationship between these values with the local conditions of the study zones as well as with the subduction setting. This is done by comparing the values calculated for different zones throughout the Chilean subduction margin with site characterization parameters V_{S30} and f_0 to see the correlation between κ, specifically its component κ_0, and the variation in the site characteristics. We also analyze the relationship between kappa, the seismic source, and path implications, in particular, the differences between in-slab and interface events.

Database and Study Area

The data used are based on the two main seismological networks throughout Chile called Chilean National Seismic Network, C, and National Seismological Network, C1. These networks have been operational since 1991 and 2012, respectively, and are under the supervision of Chile's National Seismological Center. The records used for this study are adapted from the work done by Bastías and Montalva (2016), who established a database of 3829 records from 243 seismic stations, which include seismic events from 1985 to 2015 of magnitude ranging from 4.6 to 8.8 (Fig. 1a). In addition to containing the time series, this database also has useful information for the subsequent analytical process, such as the site characterization parameters of the seismic stations (f_0 and V_{S30}), event identification (i.e., whether the event is of subduction or in-slab type), and the hypocentral and epicentral distance of the earthquake from the station.

The study area covers from the northern (Arica and Parinacota region, around 18.4° S, 70.3° W) to central–southern Chile (Biobío region, around 36.9° S, 73.0° W). Of the total number of stations in the database, only those with more than 10 records are chosen; in this way the subsequent linear fit has been shown to be more reliable to obtain κ_0 and κ_R (Ktenidou *et al.*, 2013). The final 36 stations (Fig. 1b) are distributed mainly in the north and center of the country; this is because most of the recorded seismic activity is due to the sequence of events associated with the earthquakes of Maule 2010 and Iquique 2014.

Methods

The procedure for calculating kappa follows the methodology developed by Anderson and Hough (1984). It starts by picking the *P* and *S* phases. To select the arrival time of the *P* wave the vertical component of the accelerograms is used, whereas the arrival time is selected using the horizontal component in the case of the *S* wave. This is done manually through a visual inspection of the records. The picked times are used to select the noise and signal windows of each record, marked on both horizontal components of the data. The noise window is the part of the seismic record that is selected prior to the arrival of the *P* wave, whereas the signal window is associated with the *S* wave. The length of the signal window is delimited by the times t_{S1} and t_{S2}, in which the first corresponds to the arrival time of the *S* phase and the second to the time at which the energy released during the recording of the event reaches 80% of its maximum—a value obtained through the calculation of the Arias intensity (Arias, 1970; Sotiriadis *et al.*, 2021).

The noise window is set according to the length of the signal window between times t_{P1} and t_{P2} with $t_{P1} = t_{P2} - \Delta t_S$, in which t_{P2} is the arrival time of the *P* phase selected in the signal picking, and $\Delta t_S = t_{S2} - t_{S1}$ is the length of the signal window. In the rare cases in which $t_{P2} - \Delta t_S < 0$, t_{P1} is set to zero, and the noise window has sufficient length for the subsequent analysis.

For the determination of the Fourier acceleration spectrum, a 2.5% Hanning taper is applied on both the time windows. Then, the fast Fourier transform is determined to obtain the amplitude spectrum of both the signal and the noise both horizontal components, which are combined using the root mean square (rms) to reduce the influence of the azimuthal direction in the estimation of the parameters under study (Haendel *et al.*, 2020; Ji *et al.*, 2021). Subsequently, a semiautomated process is performed to calculate kappa. The automated part follows the same procedure as Park *et al.* (2020). The steps are as follows:

1. The initial frequency $f_E = 1.5f_0$ or $f_E = 1.5f_c$ is defined, in which f_0 is the fundamental frequency and f_c is the corner frequency, estimated from the displacement spectrum. If $f_0 \geq f_c$ then f_0 is used, otherwise f_c is used.
2. The final frequency is defined to the lowest frequency of either $f_X = 0.8f_N$ or $f_X = f_{\mathrm{SNR}\leq 3}$, in which $f_{\mathrm{SNR}\leq 3}$ is the frequency at which the signal-to-noise ratio (SNR) of the spectra is less than or equal to three, and f_N is the Nyquist frequency.
3. It is verified that the condition $\Delta f = f_X - f_E > 10$ is satisfied. Otherwise, the event is not further considered.
4. An iterative process is performed for different values of f_E, with frequencies between $f_{Ei} = f_E$ and $f_{Ei} = f_X - 10$, with values incrementing by 0.5 every iteration.

Downloaded from http://pubs.geoscienceworld.org/ssa/srl/article-pdf/94/1/385/5756885/srl-2022018.1.pdf
by Universidad de Concepcion, gmontalva

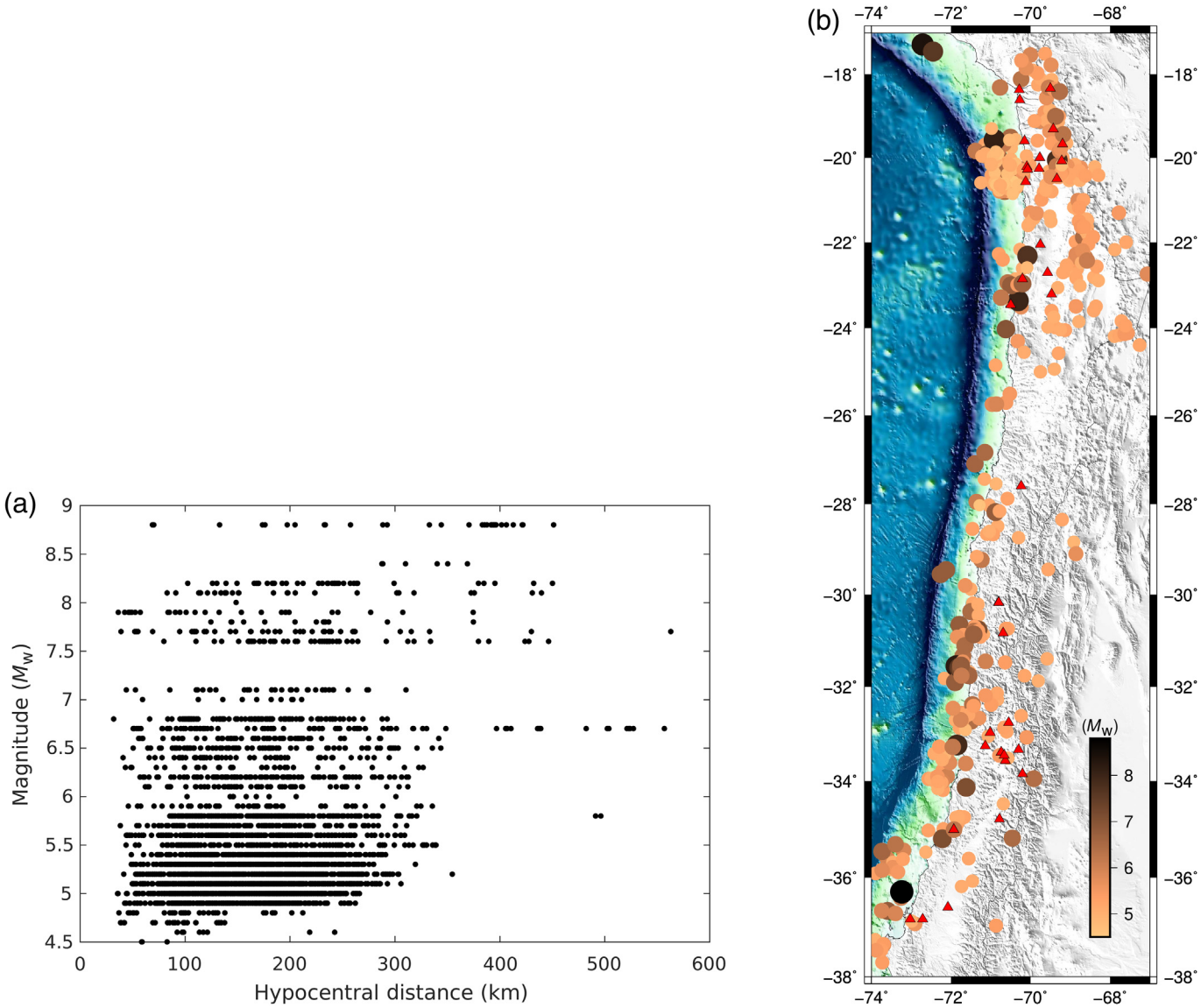

Figure 1. (a) Distribution of each record magnitude with respect to hypocentral distance. (b) Distribución of the stations (triangles) and event epicenters (circles) to be used from the database (Bastías and Montalva, 2016) throughout Chile. The color version of this figure is available only in the electronic edition.

5. Within this loop another iteration is done, but for different f_X values, which are all frequencies between $f_{Xj} = f_E + 10$ and $f_{Xj} = f_X$, and again a 0.5 increment.
6. For each pair of frequencies f_{Ei} and f_{Xj}, the linear fit of the spectrum between them is performed.
7. The optimal frequency band that provides the best fit is chosen by taking the solution giving the lowest value of the following parameter:

$$P = \frac{\text{Rms}}{\Delta f}, \tag{2}$$

in which Rms is the root mean square error between the fit and the spectrum, and Δf is the frequency band.

This process is performed for each event, and the obtained results are checked manually, verifying the frequencies f_E and f_X, while taking into consideration the relationship between frequency and magnitude. As an example of this revision, we show the case of the station CCSP (see Fig. 2a), which has a significant number of events (>20) only of the interplate type. The results for this station have a standard deviation of 0.0117, and a correlation between hypocentral distance and κ equal to 0.4198. There are five events that are close to the upper 95% confidence interval (numbers 7, 10, 11, 18, and 26 in Fig. 3a). Figure 4a shows an event (number 7 in Fig. 3a) with magnitude M_w 5.5 and is located 107 km southwest of the station. The figure shows that for the frequencies between which the acceleration spectrum decays linearly there is a steep slope

Downloaded from http://pubs.geoscienceworld.org/ssa/srl/article-pdf/94/1/385/5756885/srl-2022018.1.pdf
by Universidad de Concepcion, gmontalva

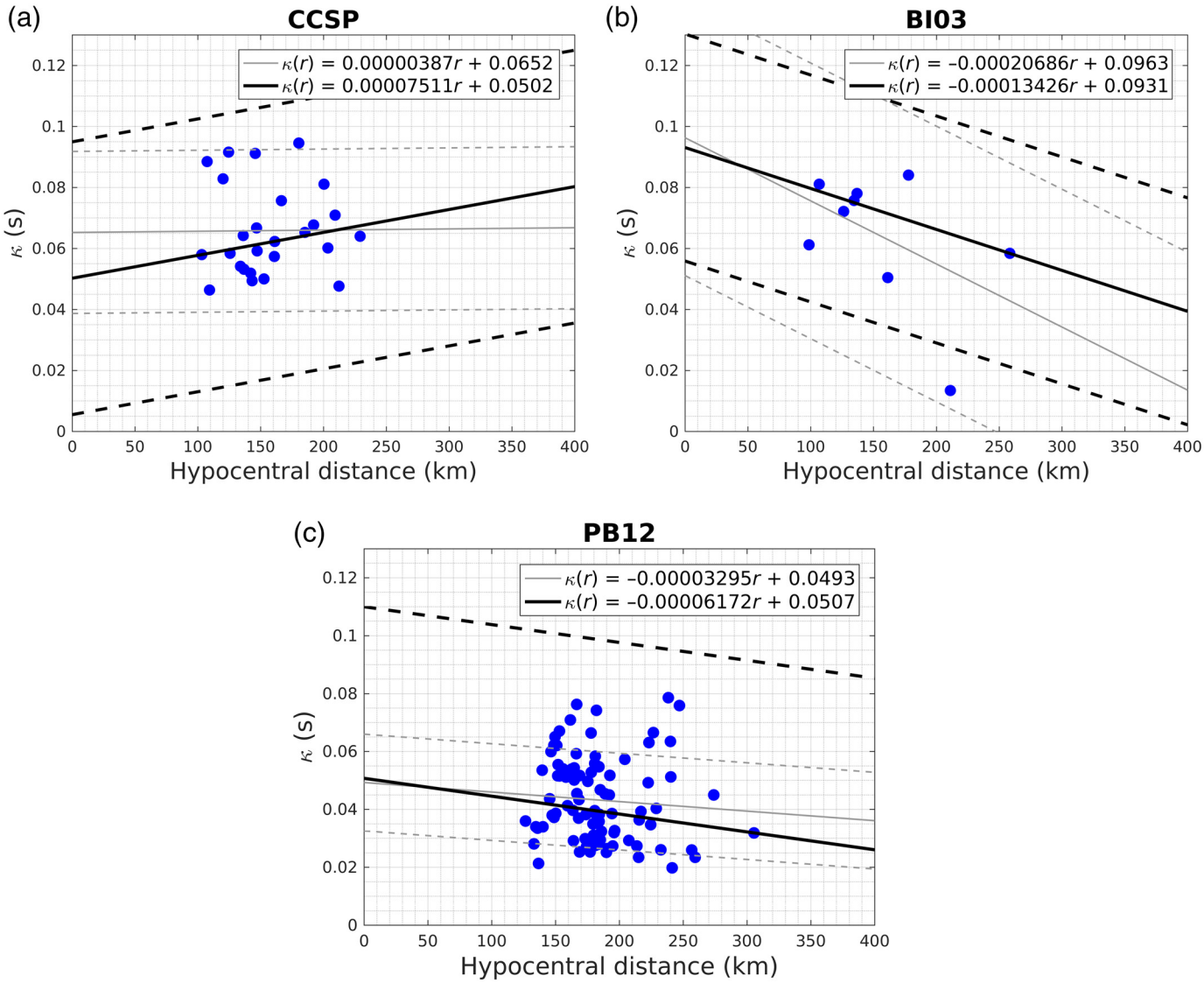

Figure 2. (a) Linear fit of the values of κ with respect to the hypocentral distance for the station CCSP (San Pedro de la Paz). The continuous black line corresponds to the robust regression, and the gray line corresponds to the linear fit obtained by least squares, with their respective confidence intervals. (b) Bad fitting for station BI03 (Biobío) due to the sparse available data point. (c) Case of station PB12 (Arica), data obtained are very scattered and cause a mismatch of the regression with respect to the expected model. The color version of this figure is available only in the electronic edition.

that leads to the value of κ calculated being high (approximately 0.09) for the given station and distance. However, following the relationship obtained between the magnitude of the event and the frequency f_E (Fig. 3c), this event is outside the trend. Then, using the relationship between magnitude and initial decay frequency (f_E), the selection of this frequency is made again, as shown in Figure 3b, presenting a new decay range between frequencies of 11.89 and 25.38 Hz. This same visual reanalysis is performed for the other stations, considering the relationship between magnitude and frequency f_E, in which the greater the magnitude of the event the smaller the frequency at which the spectrum begins to decay. This agrees with other studies that have shown a similar relationship between magnitude and f_E (Tsai *et al.*, 2000; Ktenidou *et al.*, 2013; Tsurugi *et al.*, 2020), in which magnitude is also considered as an important factor when selecting the frequency at which the spectrum begins its linear decay.

Finally, after the review, the generalized model of kappa as a function of source-to-station hypocentral distance, given by equation (1), is used to calculate κ_0 and κ_R. Before performing the linear regression a selection of the events that generate nonlinearity is made, because these cause kappa values to be higher (Ji *et al.*, 2021). The criteria for defining a linear behavior are:

- A strain index ($\gamma_{\mathrm{Ind}} = \mathrm{PGV}_{\mathrm{surf}}/V_{S30}$, with $\mathrm{PGV}_{\mathrm{surf}}$ the highest value of the recorded ground velocity) less than 0.01% (Xu *et al.*, 2020) and peak ground acceleration less than 0.25 $\mathrm{m/s^2}$ (Ji *et al.*, 2021).

Downloaded from http://pubs.geoscienceworld.org/ssa/srl/article-pdf/94/1/385/5756885/srl-2022018.1.pdf
by Universidad de Concepcion, gmontalva

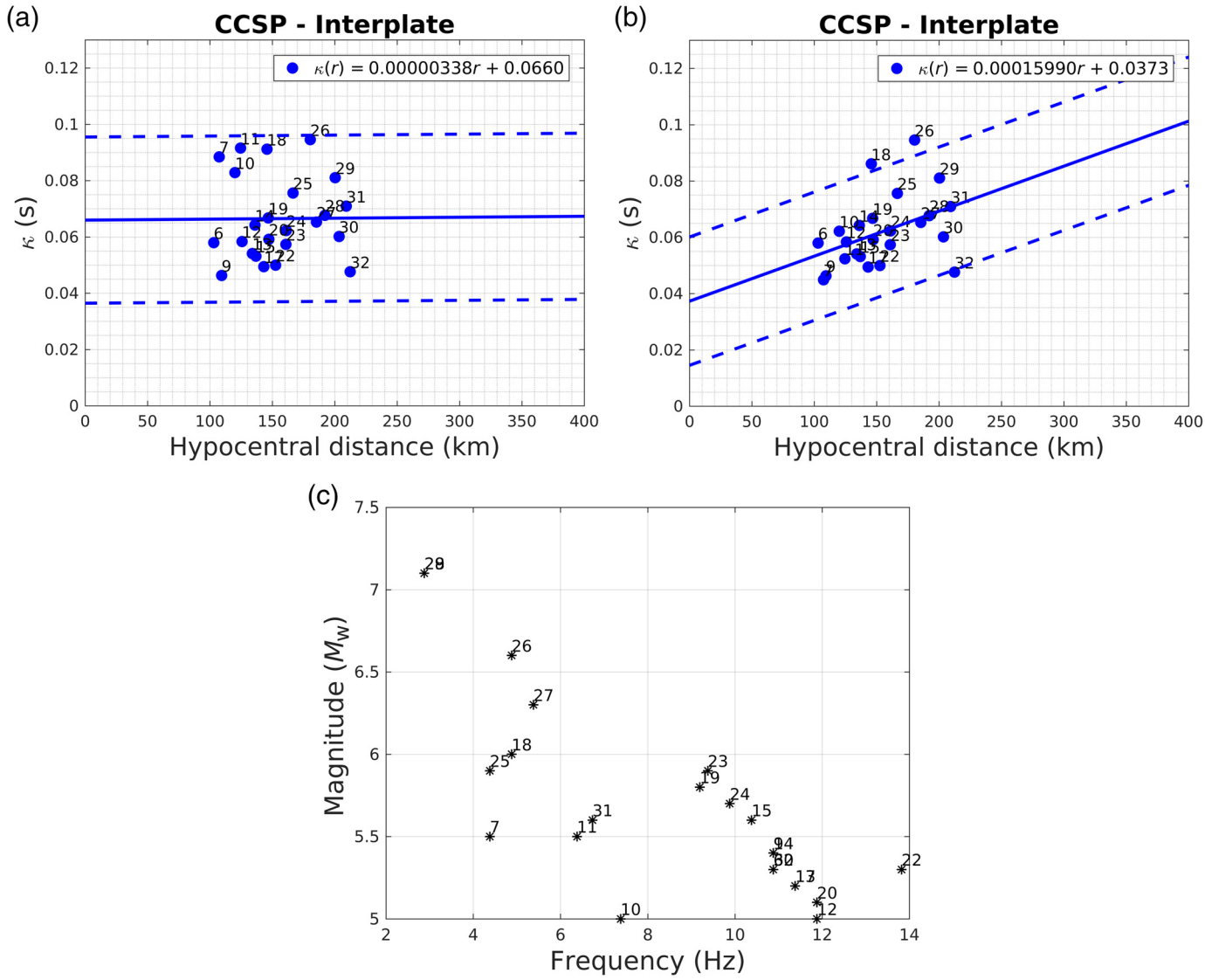

Figure 3. (a) Linear fit (L2) of the values of κ for interplate events in the station CCSP and (b) new kappa model for interplate events in the CCSP station after applying the correction to events 7, 10, 11, and 18. (c) Relation between magnitude of the event and frequency f_E for this station. Numbers next to data points correspond to the event numbers for each station. The color version of this figure is available only in the electronic edition.

In this way the κ_0 and κ_R components are calculated using two different types of regressions: the L1-norm or least absolute deviations for all source types and L2-norm or least squares for segregated sources.

For site characterization, we use the values of V_{S30} and f_0 reported by Bastías and Montalva (2016) and Leyton *et al.* (2018).

Results

The estimate of κ, and its respective components follows the methodology developed by Anderson and Hough (1984), which has been implemented in most studies on this parameter (Douglas *et al.*, 2010; Ktenidou *et al.*, 2013; Lai *et al.*, 2016). The values of κ_0 and κ_R obtained for each station are shown in Table 1, which also shows the number of events recorded at each station and its location. These values are obtained through the maximum likelihood. The result for κ_0, following the linear model (equation 1) proposed by Anderson and Hough (1984), represents the value of κ extrapolated to zero distance, that is, the value at the station site, whereas κ_R represents the distance-dependent contribution to κ from the event to the station and characterizes the slope of the fit, as shown in Figure 2a, in which the model obtained for station CCSP is presented. The validity of the regressions is limited upon available data, and the maximum distance per station is indicated in Table 1.

In certain cases, either because of the scatter in the values or because of the small number of values that remained after applying the previously explained SNR criteria, the values of κ_0 and κ_R obtained were not within the expected ranges, that is to say, values of κ_0 between 0 and 0.1 and κ_R positive. Shown is the case of the station BI03 (Fig. 2b), after the elimination of

Downloaded from http://pubs.geoscienceworld.org/ssa/srl/article-pdf/94/1/385/5756885/srl-2022018.1.pdf
by Universidad de Concepcion, gmontalva

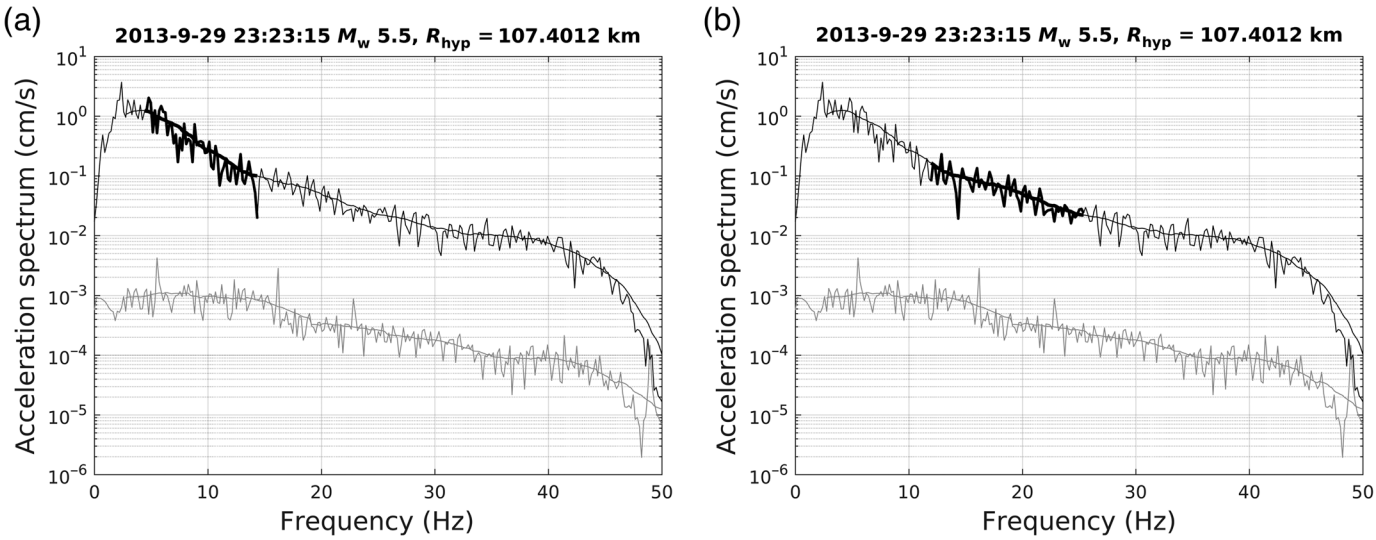

Figure 4. (a) Acceleration spectrum for an interplate event recorded at CCSP station (event number 7). In black the acceleration spectrum and in bold line the selected linear decay window are shown. The frequency limits are $f_E = 4.38$ Hz and $f_X = 14.38$ Hz. In light gray the acceleration spectrum of the pre-event noise window is shown. (b) Fourier acceleration spectrum for the signal window (black) and for the pre-event noise (gray). In addition, the new spectral decay window (gray) between $f_E = 11.89$ Hz and $f_X = 25.38$ Hz selected from the relation between magnitude and frequency.

records by the application of the SNR and nonlinearity criteria, nine events remained, so it is not possible to have a reliable inversion, as suggested by Ktenidou *et al.* (2013), who proposes that the minimum of 10 events is required. Alternatively, for the case of station PB12 (Fig. 2c) a positive value of κ_0 was obtained; however, scatter in the data gives a negative value for κ_R, which contradicts the proposed model. From this latter case an analysis was made considering the origin of the events according to their hypocenter and focal mechanism separating the records that came from interplate events from those of in-slab origin. The classification of earthquakes according to their origin is made by Bastías and Montalva (2016) based on the Centroid Moment Tensor focal mechanisms and the hypocentral location of the events. Interplate events are associated with reverse faulting with hypocenters up to 2.5° to the east of the trench and the maximum depth of 50 km. In-slab events have depths greater than 50 km and are located farther than 2.5° from the trench.

Considering the two types of events, the same analysis was extended separately for all stations, obtaining the results shown in Tables 2 and 3. Here, the data are not so scattered, because they are separated by the earthquake classification.

Discussion

The calculated values range from 0.016 to 0.075 s for κ_0, and for κ_R results are in the order of 10^{-4} to 10^{-5} s/km, which coincide with those obtained Biobío region in Chile (e.g., Neighbors *et al.*, 2015) and are in the expected range when compared with values obtained in other regions (Van Houtte *et al.*, 2011; Lai *et al.*, 2016). The longest R_{hyp} used is 400 km. Although the uniqueness of Q is likely violated by considering distances larger than 150 km (as it would also be in many cases even when using less than 150 km, as the variation of Q in the geological units of a subduction zone is on a lengthscale much less than 150 km), it allows to deal with enough data for several stations to compute kappa. Rms at different distance bins show no bias when using larger distances.

Comparison of κ for interplate and in-slab events

All the stations used in the study and the respective calculated values of κ show that the model proposed by Anderson and Hough (1984) (equation 1) works well for both in-slab and interplate earthquakes. The values of κ_0, determined for the two types of events, are not statistically different (mean difference is 0.00083, t-stat 0.903, $t_{\text{cr two-tail}}2$) for 30 stations for which κ_0 values were obtained for both types of earthquakes. The in-slab type events κ_0 values tend to be smaller than for the case of the interplate events (see Fig. 5). This was also found by Ktenidou *et al.* (2013), who compared the values of κ for subduction events with events that occurred in the crust, determining that events with greater depth had lower values of κ. Some in-slab models should be verified with more data to verify these findings.

On the other hand, the slopes of the linear fits obtained for each station, for each type of earthquake, present a clear difference between them, that is, there is a variation of the component associated with the wave path, κ_R. For interplate events the κ_R values are higher than for in-slab events, which are events that occur at a greater depth in the subducting Nazca plate in the case of this study. These lower values of κ_R for in-slab events can be explained by the increase in the value of Q at greater depths (Van Houtte *et al.*, 2011). Thus, the wave propagation for in-slab events originating inside the subducting plate

Downloaded from http://pubs.geoscienceworld.org/ssa/srl/article-pdf/94/1/385/5756885/srl-2022018.1.pdf
by Universidad de Concepcion, gmontalva

TABLE 1
Values of κ_0 and κ_R Obtained for Each Station

Station	V_{S30} (m/s)	Latitude (°)	Longitude (°)	*N* Records	Maximum Distance (km)	κ_0 (s)	κ_R (s/km)
AP01	355	−18.3708	−70.3419	70	293	0.058	0.00001923
PB12	599	−18.6141	−70.3281	89	305	0.051	−0.00006172
PB13	510	−18.3359	−69.5016	17	269	0.057	−0.00000632
T11A	346	−19.3124	−69.4273	28	400	0.053	−0.00005335
T10A	336	−19.9954	−69.767	45	400	0.038	−0.00000874
GO01	973	−19.6685	−69.1942	90	316	0.057	0.00023215
T09A	1584	−19.5957	−70.2109	10	169	0.012	0.00014141
T12A	732	−20.0707	−69.2172	13	182	−0.006	0.00033606
TA01	566	−20.5656	−70.1807	83	265	0.067	−0.00012584
T13A	378	−20.4963	−69.3375	17	228	0.058	−0.00014154
T07A	326	−20.2562	−69.7859	50	400	0.058	−0.00000147
T05A	1020	−20.2098	−70.1502	20	151	0.025	0.00002688
TA02	489	−20.2704	−70.1311	25	254	0.063	−0.00011208
PB03	711	−22.0485	−69.7531	79	309	0.016	0.00008188
PB06	736	−22.7058	−69.5719	77	376	0.006	0.00014789
PB05	773	−22.8528	−70.2024	39	373	0.009	0.00011721
PB15	532	−23.2083	−69.4709	38	355	0.012	0.00007940
PB10	790	−23.5134	−70.5541	46	400	0.055	0.00003221
GO02	820	−25.1626	−69.5904	11	338	0.064	−0.00000848
GO03	908	−27.5937	−70.2347	18	336	0.033	−0.00001488
TLL	1003	−30.1696	−70.8054	15	265	0.021	0.00008948
GO04	405	−30.1727	−70.7993	30	295	0.048	0.00008616
CO03	704	−30.8389	−70.6891	7	251	0.005	0.00017845
VA03	485	−32.7637	−70.5508	11	255	0.052	0.00010649
ROC1	1951	−32.9759	−71.0156	51	297	0.047	0.00001255
MT02	923	−33.2591	−71.1377	13	289	0.037	−0.00008515
FAR1	681	−33.3377	−70.2994	28	275	0.019	0.00011665
LMEL	808	−33.8476	−70.2034	30	287	0.045	0.00011123
MT05	496	−33.3919	−70.7381	11	273	0.076	−0.00012444
ANTU	621	−33.5691	−70.6335	31	242	0.036	0.00002185
DG01	298	−33.4563	−70.6624	16	269	0.053	0.00002272
BO02	553	−34.7924	−70.7814	10	279	0.073	−0.00006234
GO05	536	−35.0099	−71.9303	31	287	0.066	−0.00010849
CCH2	403	−36.603	−72.0778	37	301	0.073	0.00010649
BI03	269	−36.8438	−73.0258	9	259	0.0931	−0.00013426
CCSP	236	−36.8442	−72.7112	26	229	0.05	0.00007511

Selected stations are ordered by regions: Arica and Parinacota, Tarapacá, Antofagasta, Atacama, Coquimbo, Valparaíso, Santiago, O'Higgins, Maule, and Biobío, respectively. The record numbers correspond to the total for the respective station. The maximum distance refers to the largest distance for which data at each station are available.

Downloaded from http://pubs.geoscienceworld.org/ssa/srl/article-pdf/94/1/385/5756885/srl-2022018.1.pdf
by Universidad de Concepcion, gmontalva

TABLE 2
List of Values of κ_0 and κ_R Calculated from Interplate Source Events with Their Respective 95% Confidence Intervals

Station	V_{S30} (m/s)	*N* Interplate	κ_0 Interplate (s)	κ_R Interplate (s/km)
AP01	355	64	0.036 ± 0.026	0.00014705 ± 0.00012865
PB12	599	65	0.040 ± 0.023	0.00004208 ± 0.00012540
PB13	510	0	–	–
T11A	346	23	0.016 ± 0.043	0.00022454 ± 0.00025761
T10A	336	40	0.016 ± 0.018	0.00020437 ± 0.00015535
GO01	973	66	0.043 ± 0.026	0.00033408 ± 0.00013946
T09A	1584	9	0.016 ± 0.028	0.00010499 ± 0.00032064
T12A	732	10	−0.024 ± 0.072	0.00048004
TA01	566	66	0.046 ± 0.011	0.00009263 ± 0.00010382
T13A	378	14	0.024 ± 0.033	0.00009581 ± 0.00020335
T07A	326	46	0.026 ± 0.024	0.00023083 ± 0.00020042
T05A	1020	17	0.026 ± 0.011	0.00002894 ± 0.00013135
TA02	489	17	0.043 ± 0.024	0.00009606 ± 0.00023846
PB03	711	39	0.032 ± 0.014	0.00002872 ± 0.00006241
PB06	736	17	0.024 ± 0.017	0.00013611 ± 0.00007058
PB05	773	14	0.031 ± 0.018	0.00006246 ± 0.00007050
PB15	532	6	0.024 ± 0.022	0.00007684 ± 0.00007670
PB10	790	9	0.066 ± 0.024	0.00002842 ± 0.00008132
GO02	820	1	–	–
GO03	908	7	0.030 ± 0.017	0.00004868 ± 0.00008424
TLL	1003	7	0.018 ± 0.019	0.00015958 ± 0.00010390
GO04	405	14	0.055 ± 0.014	0.00008115 ± 0.00007836
CO03	704	3	0.015 ± 0.023	0.00015543 ± 0.00012105
VA03	485	5	0.053 ± 0.046	0.00014657 ± 0.00026006
ROC1	1951	40	0.040 ± 0.007	0.00006254 ± 0.00004405
MT02	923	7	0.018 ± 0.022	0.00009528 ± 0.00017466
FAR1	681	21	0.029 ± 0.023	0.00007164 ± 0.00011735
LMEL	808	20	0.033 ± 0.065	0.00020992 ± 0.00033296
MT05	496	6	0.032 ± 0.049	0.00019526 ± 0.00029461
ANTU	621	30	0.033 ± 0.016	0.00003993 ± 0.00008979
DG01	298	8	0.084 ± 0.048	−0.00019021 ± 0.00031776
BO02	553	7	0.058 ± 0.032	0.00004952 ± 0.00016329
GO05	536	22	0.046 ± 0.013	0.00004894 ± 0.00008717
CCH2	403	34	0.075 ± 0.016	0.00007947 ± 0.00008536
BI03	269	7	0.056 ± 0.027	0.00014232 ± 0.00019780
CCSP	236	24	0.037 ± 0.023	0.00015990 ± 0.00014448

The number of records considers the signal-to-noise ratio criteria already applied. In the case of an insufficient number of records, the parameters are not specified.

Downloaded from http://pubs.geoscienceworld.org/ssa/srl/article-pdf/94/1/385/5756885/srl-2022018.1.pdf
by Universidad de Concepcion, gmontalva

TABLE 3
List of Values of κ_0 and κ_R Calculated from Events of In-Slab Origin with Their Respective 95% Confidence Intervals

Station	V_{S30} (m/s)	N In-Slab	κ_0 In-Slab (s)	κ_R In-Slab (s/km)
AP01	355	6	0.027 ± 0.048	0.00011614 ± 0.00022217
PB12	599	24	0.022 ± 0.015	0.00004486 ± 0.00007171
PB13	510	17	0.054 ± 0.021	0.00001234 ± 0.00010954
T11A	346	5	0.047 ± 0.008	−0.00004087 ± 0.00002415
T10A	336	5	0.018 ± 0.021	0.00003270 ± 0.00008058
GO01	973	24	0.052 ± 0.012	0.00004018 ± 0.00005956
T09A	1584	1	–	–
T12A	732	3	0.013 ± 0.076	0.00015964 ± 0.00050895
TA01	566	17	0.038 ± 0.008	−0.00000360 ± 0.00004026
T13A	378	3	0.059 ± 0.034	−0.00014015 ± 0.00025319
T07A	326	4	0.042 ± 0.009	−0.00000773 ± 0.00003359
T05A	1020	3	−0.071 ± 0.063	0.00072132 ± 0.00044219
TA02	489	8	0.035 ± 0.021	0.00001361 ± 0.00010697
PB03	711	40	0.023 ± 0.011	0.00001183 ± 0.00005347
PB06	736	60	0.025 ± 0.012	0.00001383 ± 0.00006286
PB05	773	25	0.025 ± 0.014	0.00001505 ± 0.00006951
PB15	532	32	0.020 ± 0.011	0.00004101 ± 0.00004538
PB10	790	37	0.059 ± 0.010	0.00000639 ± 0.00004860
GO02	820	10	0.036 ± 0.014	0.00008701 ± 0.00006404
GO03	908	11	0.022 ± 0.033	0.00001080 ± 0.00017885
TLL	1003	8	0.016 ± 0.023	0.00008001 ± 0.00010473
GO04	405	16	0.051 ± 0.019	0.00002075 ± 0.00009138
CO03	704	4	0.023 ± 0.033	0.00006866 ± 0.00017453
VA03	485	6	0.053 ± 0.023	0.00008208 ± 0.00010678
ROC1	1951	11	0.035 ± 0.019	0.00003820 ± 0.00009626
MT02	923	6	0.018 ± 0.015	−0.00000751 ± 0.00007135
FAR1	681	7	0.028 ± 0.022	0.00000592 ± 0.00012986
LMEL	808	10	0.041 ± 0.022	0.00006798 ± 0.00010848
MT05	496	5	0.043 ± 0.012	0.00000391 ± 0.00006235
ANTU	621	1	–	–
DG01	298	8	0.019 ± 0.022	0.00013112 ± 0.00011329
BO02	553	3	0.028 ± 0.001	0.00007976 ± 0.00000463
GO05	536	9	0.028 ± 0.008	0.00001678 ± 0.00004017
CCH2	403	3	0.053 ± 0.045	0.00004086 ± 0.00029350
BI03	269	2	−0.187	0.00094962
CCSP	236	2	0.032	0.00013910

Stations with only two events do not have confidence intervals. The number of records considers the signal-to-noise ratio criteria already applied. In the case of an insufficient number of records, the parameters are not specified.

Downloaded from http://pubs.geoscienceworld.org/ssa/srl/article-pdf/94/1/385/5756885/srl-2022018.1.pdf
by Universidad de Concepcion, gmontalva

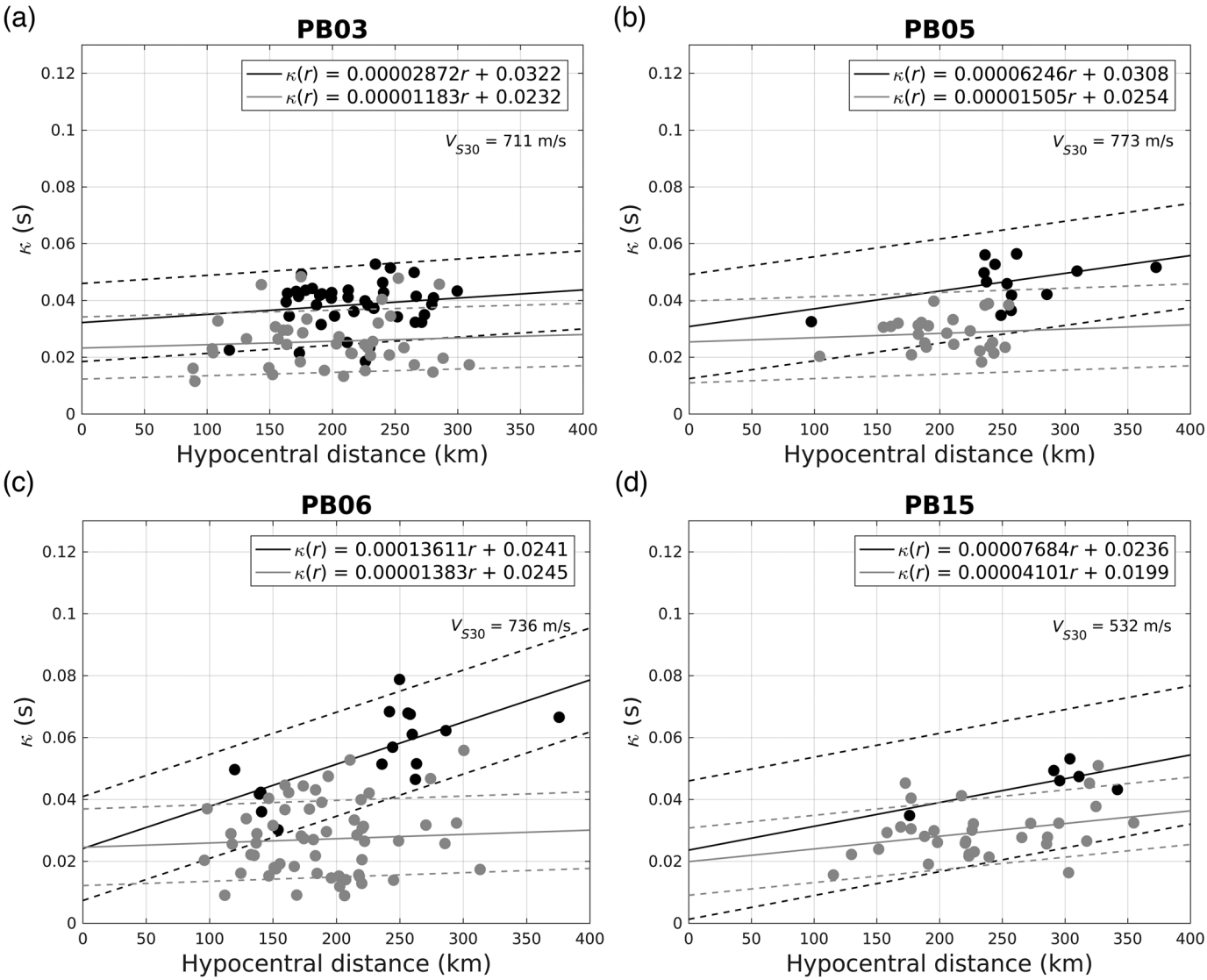

Figure 5. Values of κ obtained for some stations in the Antofagasta region. In gray are the in-slab events and κ fit, and black dots show the interplate events and their fit. (a) Station PB03, (b) Station PB05, (c) Station PB06, and (d) Station PB15.

has part of its trajectory through a medium with a high Q value, which leads to a reduced attenuation of the seismic wave in the corresponding frequency range (Lin and Lee, 2008). Although azimuthal dependencies could play a role in observing different κ_R values, there is no preferential orientation for in-slab or interplate events, and also the dataset is not big enough to split enough (>10) events into separate azimuths. Montalva *et al.* (2021) explain that, for example, splitting ground-motion residuals into different paths (i.e., path-to-path residual) has no benefit for this dataset.

Variation of the linear fit with epicentral versus hypocentral distance

Another important consideration within the analysis of κ, and even more so in an area where the main seismogenesis of earthquakes is subduction, is the distance used to make the fit of κ. Whether the hypocentral or epicentral distance is used to make the inversion, the calculated values of κ increase with distance (see Fig. 6). So, considering either of the distance metrics the Anderson and Hough (1984) model fits the data well. However, there is a variation in the site and trajectory components associated with κ depending on the distance calculation used. The results obtained using the epicentral distance present values of κ_0 greater than those determined through the hypocentral distance for interplate and in-slab earthquakes. For the interplate earthquakes the largest difference between the values of κ_0, for a particular station, was 20%, whereas for the case of the in-slab earthquakes the variation was greater, reaching values close to 35%. Ktenidou *et al.* (2013) also noted this variation in the fitting of κ, identifying that the calculated value of κ_0 was smaller when hypocentral distance instead of epicentral distance was used, whereas the component associated with the trajectory (κ_R) was similar (in our study the variation of κ_R does not exceed 8%).

Downloaded from http://pubs.geoscienceworld.org/ssa/srl/article-pdf/94/1/385/5756885/srl-2022018.1.pdf
by Universidad de Concepcion, gmontalva

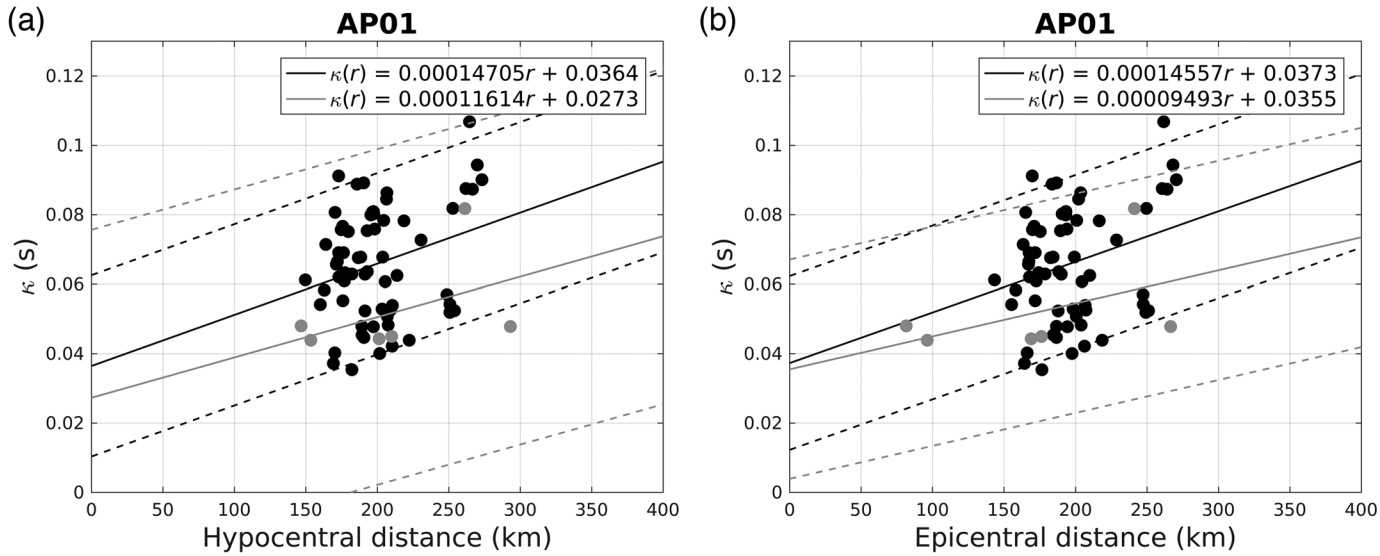

Figure 6. Difference between the linear fits obtained using (a) hypocentral and (b) epicentral distances. Results correspond to station AP01 located in the Arica region. In gray the values of κ and the linear fit of the in-slab events, and in black the case of the records of interplate events are shown.

The variation in the site component is because the epicentral distance does not incorporate the depth of the event, which causes the κ values to be closer to the origin ($R = 0$), which is in which κ_0 is determined. Hence, the linear regression of a model using R_{epi} will obtain higher κ_0 values. The fact that there is a greater difference in the case of in-slab earthquakes is because these events have a greater depth, hence, this effect is magnified.

κ_0 dependence on V_{S30} and f_0

Ktenidou *et al.* (2014) summarizes the different relationships available in the literature for V_{S30} and κ_0. The results compiled by this study follow the same trend for the one obtained in this work (Fig. 7a), in which the values of κ_0 decrease as V_{S30} increases. Following the classification of the Chilean standard (see Table 4), less consolidated soils ($V_{S30} < 400$ m/s) are associated with values of κ_0 higher than for more compact soils. This means that the seismic wave, when propagated through the surface structure associated with the site, suffers a greater attenuation at higher frequencies in softer sites.

We studied the variation of κ_0 with respect to the fundamental frequency of the site (f_0), which is associated with the deeper structure under each station. The κ_0–f_0 relation obtained is shown in Figure 7b, in which a linear fit with a negative slope is obtained for the case of the shear wave velocity, which is expected considering the results obtained in the literature by Ktenidou *et al.* (2015) and taking into account that the origin of κ is associated not only with the first 30 m considered in the calculation of V_{S30} but also with the medium to a depth of a few kilometers below the site.

Conclusions

Following the methodology of Anderson and Hough (1984), in which their linear model is used to calculate the site and path components of κ, we determined the values of this parameter at 36 stations in Chile with respect to the epicentral and hypocentral distances, obtaining results with a clear dispersion. This is more evident due to the treatment of interplate and in-slab events separately, because the path component is smaller for the in-slab events than for the interface events. Calculating the regression separately, according to the earthquake type, significantly improves the results, presenting a smaller dispersion. It should be noted that for some stations in-slab models were fitted with limited data, and that manual selection of the f_E frequency could induce a potential bias, it is necessary to review the selected frequencies, taking into account the relationship between these frequencies and the event magnitude associated with the seismic record, considering that the greater the magnitude, the lower the value of f_E.

TABLE 4
Extract from the Chilean Seismic Classification of the Foundation Site

Soil Type		V_{S30} (m/s)
A	Rock, cemented soil	≥900
B	Soft or fractured rock, very dense, or very stiff soil	≥500
C	Dense or solid soil	≥350
D	Medium dense or solid soil	≥180
E	Soil of medium compactness or consistency	<180

Supreme Decree 61 (DS61) of the Chilean Ministry of Housing and Planning (MINVU), 2011 (Guendelman *et al.*, 2012).

Downloaded from http://pubs.geoscienceworld.org/ssa/srl/article-pdf/94/1/385/5756885/srl-2022018.1.pdf
by Universidad de Concepcion, gmontalva

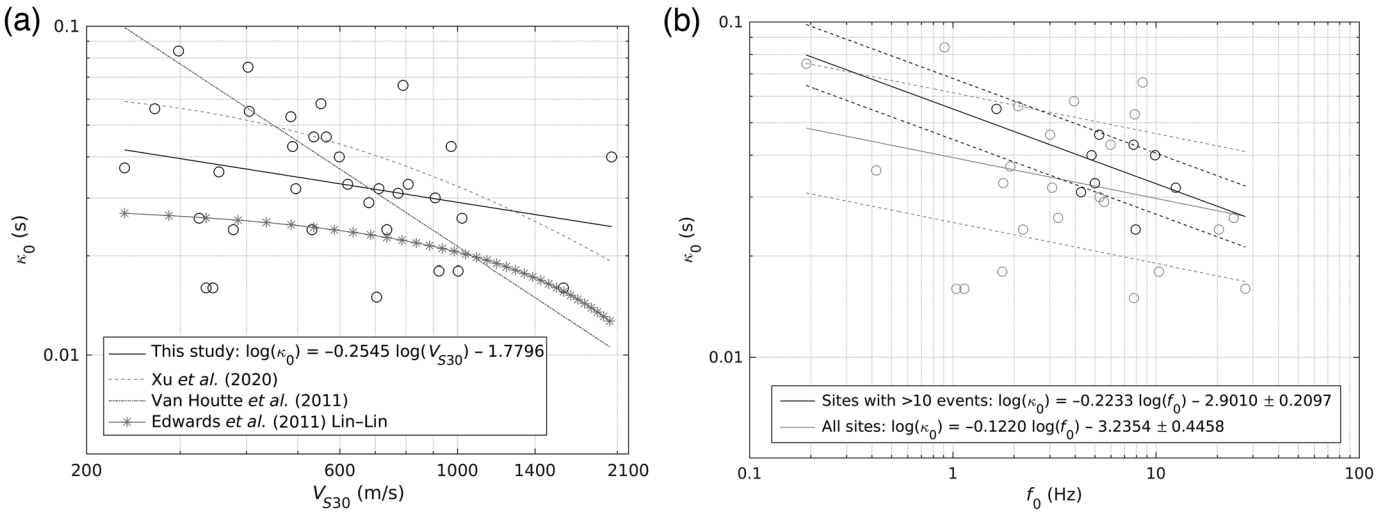

Figure 7. (a) Relationship between κ_0 and V_{S30} calculated from interplate events. This has a value of $R^2 = 0.0725$. (b) Relation between κ_0 and f_0 calculated from interplate events for sites with more than 10 events on each source, which has a value of $R^2 = 0.2850$, much greater than for the V_{S30}–κ_0 relationship.

The values of κ_0 determined for interplate events are, in general, slightly higher than those for in-slab events; nevertheless, the variation is not statistically significant, confirming that it is a site parameter. On the other hand, the values of κ_R for interplate events are higher than those of in-slab events, which is associated with lower values of Q. This implies that the events that come from greater depths (in-slab events), in which the values of Q are greater, will have less attenuation at high frequencies. Another important point is the use of the hypocentral or epicentral distance for the calculation of the κ components, because the values of κ_0 tend to be larger when using the epicentral distance. In the case of areas where the main seismic sources are subduction earthquakes, this effect is more significant due to the deeper hypocenters that some of these events have, compared with other areas of the world.

The variation of κ_0 with the site parameters V_{S30} and f_0 agrees with the relationships obtained in the previous studies, in which high values of κ_0 are associated with lower values of both V_{S30} and f_0. We provide these relations between κ_0 and site-specific parameters V_{S30} and f_0 (see Fig. 7), in which f_0 is a better predictor of κ_0 than the more commonly used V_{S30}–κ_0 relation. This can be useful for improving site terms for modern ground-motion prediction equations to make appropriate V_S-kappa corrections for site response analyses (Cabas *et al.*, 2017) or to improve soil–structure interaction studies (Sotiriadis *et al.*, 2021).

Another important observation is the variation of the kappa components (κ_0 and κ_R) throughout Chile. For the case of the κ_R component, in all regions the average of the results is in the order of 10^{-4} s/km, obtaining the highest values (greater than 2×10^{-4}) in the regions of Tarapacá (~20° S), Santiago (~33° S), and Biobío (~37° S), showing that there is no significant variation throughout the country. Regarding the variation of κ_0, it is not possible to establish a regional dependence. In contrast to other works that calculate κ_0 from the coda spectrum and a relation between κ_0 and the regional structure can be observed (Mayor *et al.*, 2018; Pilz *et al.*, 2019), in this work a major relation with the site conditions is observed. However, there is a tendency between κ_0 values and the location of the station in the east–west direction, with higher values in areas of soft sediments, as in basins or coastal areas of the country, and smaller values in places of more consolidated soils or rock as in the Andes and foothills. This coincides with the results shown in the literature about the inverse relationship between kappa and V_{S30}.

Finally, it is important to extend the study of these parameters along the whole South American subduction margin. The recent advances in instrumentation will allow this in the future once sufficient events have been recorded along the southamerican subduction zone.

Data and Resources

The seismic series were obtained from Bastías and Montalva (2016). Figures were made using MATLAB software and Generic Mapping Tools (GMT; Wessel *et al.*, 2013; http://www.soest.hawaii.edu/gmt, last accessed January 2022).

Declaration of Competing Interests

The authors acknowledge that there are no conflicts of interest recorded.

Acknowledgments

The authors acknowledge financial support from the Millennium Nucleus CYCLO (the seismic cycle along subduction zones), funded by the Millennium Scientific Initiative (ICM) of the Chilean Government Grant Number NC160025, Fondequip EQM 160015 for providing valuable data, and the Chilean Scientific and Technological Development Support Fund (FONDEF) Grant Number ID16I20157. The authors thank the thoughtful comments by Sanjay Bora and an anonymous reviewer who greatly contributed to improve the article.

Downloaded from http://pubs.geoscienceworld.org/ssa/srl/article-pdf/94/1/385/5756885/srl-2022018.1.pdf
by Universidad de Concepcion, gmontalva

References

Aki, K. (1980). Scattering and attenuation of shear waves in the lithosphere, *J. Geophys. Res.* **85,** no. B11, 6496–6504.

Anderson, J. G., and S. E. Hough (1984). A model for the shape of the Fourier amplitude spectrum of acceleration at high frequencies, *Bull. Seismol. Soc. Am.* **74,** 1969–1993.

Arias, A. (1970). A measure of earthquake intensity, in *Seismic design of nuclear power plants*, R. Hansen (Editor), M.I.T. Press, Cambridge, Massachusetts.

Bastías, N., and G. A. Montalva (2016). Chile strong ground motion flatfile, *Earthq. Spectra* **32,** no. 4, 2549–2566.

Bora, S. S., F. Cotton, F. Scherbaum, B. Edwards, and P. Traversa (2017). Stochastic source, path and site attenuation parameters and associated variabilities for shallow crustal European earthquakes, *Bull. Earthq. Eng.* **15,** no. 11, 4531–4561, doi: 10.1007/S10518-017-0167-X.

Cabas, A., A. Rodriguez-Marek, and G. A. Montalva (2015). Vs-kappa consistent input ground motions for site response analyses. Case study in Concepción and San Pedro, Chile, *15th Pan-American Conf. on Soil Mechanics and Geotechnical Engineering.*

Cabas, A., A. Rodriguez-Marek, and L. F. Bonilla (2017). Estimation of site-specific kappa (κ0)-consistent damping values at KiK-net sites to assess the discrepancy between laboratory-based damping models and observed attenuation (of seismic waves) in the field, *Bull. Seismol. Soc. Am.* **107,** no. 5, 2258–2271.

Campbell, K. W. (2003). Prediction of strong ground motion using the hybrid empirical method and its use in the development of ground-motion (attenuation) relations in eastern North America, *Bull. Seismol. Soc. Am.* **93,** no. 3, 1012–1033.

Cotton, F., F. Scherbaum, J. J. Bommer, and H. Bungum (2006). Criteria for selecting and adjusting ground-motion models for specific target regions: Application to central Europe and rock sites, *J. Seismol.* **10,** 137–156.

Darragh, R., I. Wong, and W. Silva (2019). Evaluating kappa, Q(f), and stress parameter in the southern Rocky Mountains of central Colorado, *Bull. Seismol. Soc. Am.* **109,** no. 2, 586–599.

Douglas, J., P. Gehl, L. F. Bonilla, and C. Gelis (2010). A κ model for mainland France, *Pure Appl. Geophys.* **167,** 1303–1315.

Drouet, S., F. Cotton, and P. Gueguen (2010). V_{S30}, κ, regional attenuation and M_w from accelerograms: Application to magnitude 3-5 French earthquakes, *Geophys. J. Int.* **182,** 880–898.

Fu, L., and X. J. Li (2016). The characteristics of high-frequency attenuation of shear waves in the Longmen Shan and adjacent regions, *Bull. Seismol. Soc. Am.* **106,** no. 5, 1979–1990.

Guendelman, T., G. R. Saragoni, and R. Verdugo (2012). Chilean emergency seismic design code for buildings after El Maule 2010 earthquake, *Proc. of the 15 WCEE*, paper, 4480.

Haendel, A., J. G. Anderson, M. Pilz, and F. Cotton (2020). A frequency-dependent model for the shape of the Fourier amplitude spectrum of acceleration at high frequencies, *Bull. Seismol. Soc. Am.* **110,** no. 6, 2743–2754.

Hanks, T. C. (1982). $f_{\max}$, *Bull. Seismol. Soc. Am.* **72,** 1867–1879.

Havskov, J., M. B. Sørensen, D. Vales, M. Özyazicioğlu, G. Sánchez, and B. Li (2016). Coda Q in different tectonic areas, influence of processing parameters, *Bull. Seismol. Soc. Am.* **106,** no. 3, 956–970.

Ji, C., A. Cabas, L. F. Bonilla, and C. Gelis (2021). Effects of nonlinear soil behavior on kappa (κ): Observations from the KiK-Net database, *Bull. Seismol. Soc. Am.* **111,** no. 4, 2138–2157.

Ktenidou, O.-J., C. Gelis, and F. Bonilla (2013). A study on the variability of kappa in a borehole, implications on the computation method used, *Bull. Seismol. Soc. Am.* **103,** 1048–1068.

Ktenidou, O.-J., F. Cotton, N. Abrahamson, and J. G. Anderson (2014). Taxonomy of kappa: A review of definitions and estimation approaches targets to applications, *Seismol. Res. Lett.* **85,** no. 1, 135–146.

Ktenidou, O.-J., N. A. Abrahamson, S. Drouet, and F. Cotton (2015). Understanding the physics of kappa (κ): Insights from a downhole array, *Geophys. J. Int.* **203,** 678–691.

Lai, T. S., H. Mittal, W. A. Chao, and Y. M. Wu (2016). A study on kappa value in Taiwan using borehole and surface seismic array, *Bull. Seismol. Soc. Am.* **106,** 1509–1517.

Laurendeau, A., F. Cotton, O. -J. Ktenidou, L. F. Bonilla, and F. Hollender (2013). Rock and stiff-soil site amplification: Dependencies on V_{S30} and kappa (κ_0), *Bull. Seismol. Soc. Am.* **103,** no. 6, 3131–3148.

Leyton, F., A. Leopold, G. Hurtado, C. Pastén, S. Ruiz, G. Montalva, and E. Saéz (2018). Geophysical characterization of the Chilean seismological stations: First results, *Seismol. Res. Lett.* **89,** no. 2A, 519–525, doi: 10.1785/0220170156.

Lin, P. S., and C. T. Lee (2008). Ground-motion attenuation relationships for subduction zone earthquakes in northeastern Taiwan, *Bull. Seismol. Soc. Am.* **98,** no. 1, 220–240.

Mayor, J., S. S. Bora, and F. Cotton (2018). Capturing regional variations of hard-rock κ_0 from coda analysis, *Bull. Seismol. Soc. Am.* **108,** no. 1, 399–408, doi: 10.1785/0120170153.

Montalva, G. A., N. Bastías, and F. Leyton (2021). Strong ground motion prediction model for PGV and spectral velocity for the Chilean subduction zone, *Bull. Seismol. Soc. Am.* **112,** 348–360, doi: 10.1785/0120210037.

Neighbors, C., E. J. Liao, E. S. Cochran, G. J. Funning, A. I. Chung, J. F. Lawrence, C. Christensen, M. Miller, A. Belmonte, and H. H. Andres Sepúlveda (2015). Investigation of the high-frequency attenuation parameter, κ (kappa), from aftershocks of the 2010 Mw 8.8 Maule, Chile earthquake, *Geophys. J. Int.* **200 ,** 200–215.

Park, S. J., J. M. Lee, and C.-E. Baag (2020). Estimation of high-frequency spectral decay (κ) for the Gyeongju area in south Korea, *Bull. Seismol. Soc. Am.* **110,** no. 1, 295–311.

Pilz, M., and D. Fäh (2017). The contribution of scattering to near-surface attenuation, *J. Seismol.* **21,** 1–19.

Pilz, M., F. Cotton, R. Zaccarelli, and D. Bindi (2019). Capturing regional variations of hard-rock attenuation in Europe, *Bull. Seismol. Soc. Am.* **109,** no. 4, 1401–1418, doi: 10.1785/0120190023.

Silva, W. J., and R. Darragh (1995). *Engineering Characterization of Earthquake Strong Ground Motion Recorded at Rock Sites*, Electric Power Research Institute, Palo Alto, TR-102261.

Sotiriadis, D., B. Margaris, N. Klimis, and A. Sextos (2021). Implications of high-frequency decay parameter, "κ-kappa", in the estimation of kinematic soil-structure interaction effects, *Soil Dynam. Earthq. Eng.* **144,** 106,665.

Toro, G. R., N. A. Abrahamson, and J. F. Schneider (1997). Model of strong ground motions from earthquakes in central and eastern North America: Best estimates and uncertainties, *Seismol. Res. Lett.* **68,** 41–57.

Tsai, C-C., P. Tsai, and K-C. Chen (2000). A model for the high-cut process of strong-motion accelerations in terms of distance,

Downloaded from http://pubs.geoscienceworld.org/ssa/srl/article-pdf/94/1/385/5756885/srl-2022018.1.pdf
by Universidad de Concepcion, gmontalva

magnitude, and site condition: An example from the SMART 1 array, Lotung, Taiwan, *Bull. Seismol. Soc. Am.* **90,** no. 6, 1535–1542.

Tsurugi, M., R. Tanaka, T. Kagawa, and K. Irikura (2020). High-frequency spectral decay characteristics of seismic records of inland crustal earthquakes in Japan: Evaluation of the $f_{\max}$ and κ models, *Bull. Seismol. Soc. Am.* **110,** no. 2, 452–470.

Van Houtte, C., C. Drouet, and F. Cotton (2011). Analysis of the origins of κ (kappa) to compute hard rock to rock adjustment factors for GMPEs, *Bull. Seismol. Soc. Am.* **101,** 2926–2941.

Wessel, P., W. H. F. Smith, R. Scharroo, J. Luis, and F. Wobbe (2013). Generic mapping tools: Improved version released, *Eos Trans. AGU* **94,** no. 45, 409.

Xu, B., E. M. Rathje, Y. Hashash, J. Stewart, K. Campbell, and W. J. Silva (2020). $\kappa_0$for soil sites: Observations from KiK-net sites and their use in constraining small-strain damping profiles for site response analysis, *Earthq. Spectra* **36,** no. 1, 111–137.

Manuscript received 13 January 2022
Published online 30 September 2022

Downloaded from http://pubs.geoscienceworld.org/ssa/srl/article-pdf/94/1/385/5756885/srl-2022018.1.pdf
by Universidad de Concepcion, gmontalva